THE JOURNAL OF PHYSICAL CHEMISTRY C

Article

Cite This: J. Phys. Chem. C 2019, 123, 1519−1526

pubs.acs.org/JPCC

Understanding the Formation of Conductive Mesocrystalline Superlattices with Cubic PbS Nanocrystals at the Liquid/Air Interface

Santanu Maiti,*[,†] Sonam Maiti,[†,‡] Andre Maier,[‡] Jan Hagenlocher,[†] Andrei Chumakov,[§] Frank Schreiber,*[,†,∥] and Marcus Scheele*[,‡,∥]

[†]Institute of Applied Physics, University of Tübingen, Auf der Morgenstelle 10, 72076 Tübingen, Germany

[‡]Institute of Physical and Theoretical Chemistry, University of Tübingen, Auf der Morgenstelle 18, 72076 Tübingen, Germany

[§]Beamline ID10, European Synchrotron Radiation Facility (ESRF), F-38043 Grenoble, France

[∥]Center for Light-Matter Interaction, Sensors & Analytics LISA+, University of Tübingen, Auf der Morgenstelle 15, 72076 Tübingen, Germany

Supporting Information

ABSTRACT: We report the formation of conductive mesocrystalline superstructures of cubic PbS nanocrystals (NCs) through directional cross-linking with organic semiconductors at the liquid/air interface monitored simultaneously by in situ grazing incidence small angle X-ray scattering and grazing incidence X-ray diffraction. We determine the superlattice type, its symmetry and parameters, and the atomic orientation of NCs from the time-resolved scattering patterns. The superlattice contraction follows an exponential decay during ligand exchange, preserving always the two-dimensional square geometry. We attribute the contraction to the continuous replacement of oleic acid with smaller cobalt/copper 4,4′,4″,4‴-tetraaminophthalocyanine molecules. In these superlattices, the NCs are directed with a $[100]_{AL}$ axis perpendicular to the liquid surface for the whole assembly period. The kinetics and structural results provide a direct correlation between the superstructure and their atomic orientation on the liquid surface during self-assembly followed by ligand exchange.

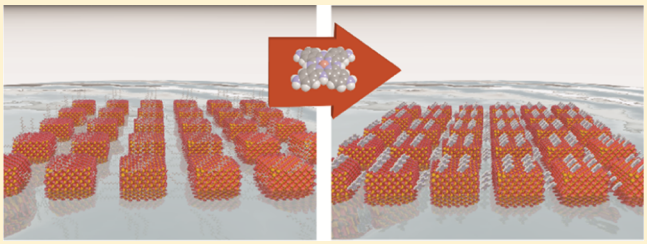

INTRODUCTION

Spontaneous and directed self-assembly of inorganic nanocrystals (NCs) into ordered arrangements is a fascinating field of nanoscience.[1−7] In most cases, the superlattices (SLs) with the as-prepared NCs are poorly conductive because of their insulating surface ligand shell. Electronically, coupled organic−inorganic nanostructures consisting of inorganic NCs and organic semiconductor (OSC) molecules are a novel class of hybrid materials which show interesting transport and optoelectronic properties.[8−10] The physical properties of the assembled hybrid two-dimensional (2D) nanostructures can be further tuned by the size and shape of their constituents as well as their structural order.[11−13] Therefore, a key challenge for conductive NC ensembled with tailored charge transport is the assembly into SLs with defined long-range order and orientation.[5,14−16] Langmuir-type assembly of colloidal NCs passivated with organic surface ligands at the liquid/air interface leads to a monolayer of cross-linked films with a long-range order.[17,18] NC SLs with mesocrystalline ordering, for example the atomic lattice (AL) of all individual NCs in the superstructure are aligned along a specific crystallographic axis, which enables the study of direction/orientation-dependent charge transport.[19,20] Recent advances in computational work also predict that the iso-oriented mesocrystalline assembly of NCs holds for favorable optoelectronic properties for applications in light-emitting diodes, photodetectors, or solar cells.[21,22] OSC molecules have a preference to bind a certain facet of the NCs and replace the native oleic acid (OA) ligands of the NCs.[23] Cross-linking of small OSCs with NCs produces macroscopic domains of long range-ordered coupled nanostructures, but the exact formation mechanism of conductive iso-oriented mesocrystalline superstructure is still unknown.[24]

Here, we choose the organic pi-system cobalt β-tetraaminophthalocyanine (CoTAPc) to ligand exchange and crosslink OA-capped cubic PbS NCs (edge length 10.9 ± 1.4 nm) into a conductive SL. To study its formation, we monitor in situ the evolution of the SL at the acetonitrile/air interface in real-time by grazing incidence small angle X-ray scattering (GISAXS) and grazing incidence X-ray diffraction (GIXD) simultaneously. The kinetics of this ligand exchange is compared to a second experiment using the analogous copper phthalocyanine (CuTAPc).[25] By GISAXS, one can determine the structure, orientation, and symmetry of the SL assembly, whereas GIXD provides the information on preferential orientation of the ALs of the NCs within the SLs (details are provided in the Supporting Information).[26−30] For simplicity, we denote the

Received: November 29, 2018
Revised: December 5, 2018
Published: December 17, 2018

DOI: 10.1021/acs.jpcc.8b11518
J. Phys. Chem. C 2019, 123, 1519−1526

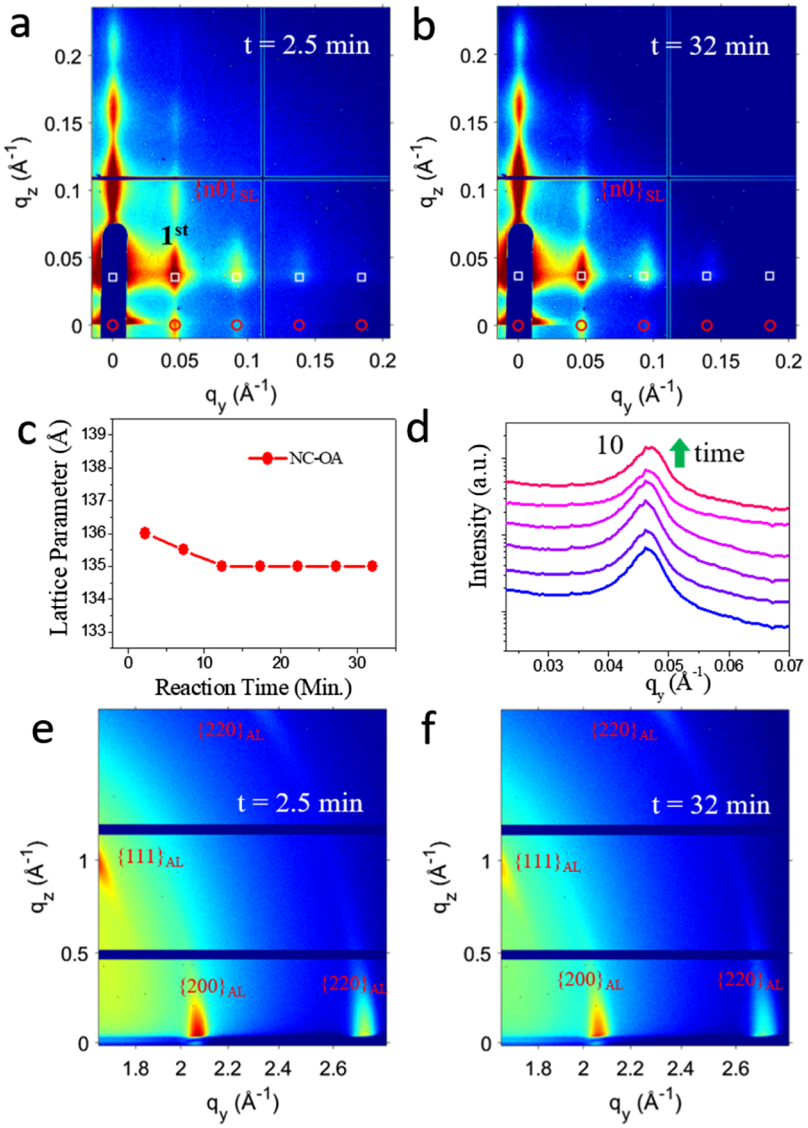

Figure 1. Self-assembly of cubic PbS NCs. GISAXS patterns of the NCs for a waiting period of (a) 2.5 and (b) 32 min after injection onto the acetonitrile surface and consecutive solvent evaporation. The red circles and white boxes are the simulated diffraction patterns considering a square SL (space group: *P4mm*) along the in-plane direction. (c) Temporal evolution of the lattice parameter of the 2D square unit cell, extracted by fitting each image with suitable unit cell parameters with elapsed time. (d) In-plane line profiles along q_y through the $\{n_0\}$ truncation rods of the GISAXS patterns obtained during self-assembly. GIXD patterns of the NCs for (e) 2.5 and (f) 32 min of waiting time after injection onto the liquid surface.

AL of NCs and SL of the superstructure with the subscripts "AL" and "SL", respectively, throughout the text. The NCs self-assemble into a 2D square SL monolayer within a minute after their injection on the liquid surface. The SL parameters remain almost constant during this self-assembly process. The NCs within the SL are preferentially oriented along the $[100]_{AL}$ axis perpendicular to the liquid surface, which remains unaltered during the rest of the assembling period. A continuous in-plane contraction of the lattice parameter occurs during ligand exchange by replacing OA with the smaller OSC molecules. For both cases, the shrinkage of the in-plane lattice parameters as a function of elapsed time follows an exponential decay and finally reaches similar interparticle (nearest-neighbor) distances. The appearance of similar atomic diffraction spots at the same q-positions in the time-resolved GIXD patterns, collected during ligand exchange, suggests that the ligands spontaneously bind to the $\{100\}_{AL}$–$\{100\}_{AL}$ facets of the alternating NCs without altering their atomic orientations. The combined results of GISAXS and GIXD confirm the formation of an iso-oriented mesocrystalline superstructure of PbS NCs.

METHODS

Preparation of Cubic PbS NCs. The PbS NCs were prepared according to the method previously reported by Weidmann et al.[31] The prepared NCs (TEM image in Figure S7) are precipitated by adding anhydrous ethanol to the colloidal solution. The suspension is centrifuged at 4000 rpm for 5 min. After discarding the supernatant, the centrifugate is dissolved in anhydrous hexane. The washing procedure is repeated two more times and the NCs are finally stored in anhydrous hexane. The whole synthesis procedure is carried out under inert conditions.

Synthesis of Co/CuTAPc. CuTAPc was synthesized in two steps following Jung et al.[32] CoTAPc was purchased from abcr

DOI: 10.1021/acs.jpcc.8b11518
J. Phys. Chem. C 2019, 123, 1519−1526

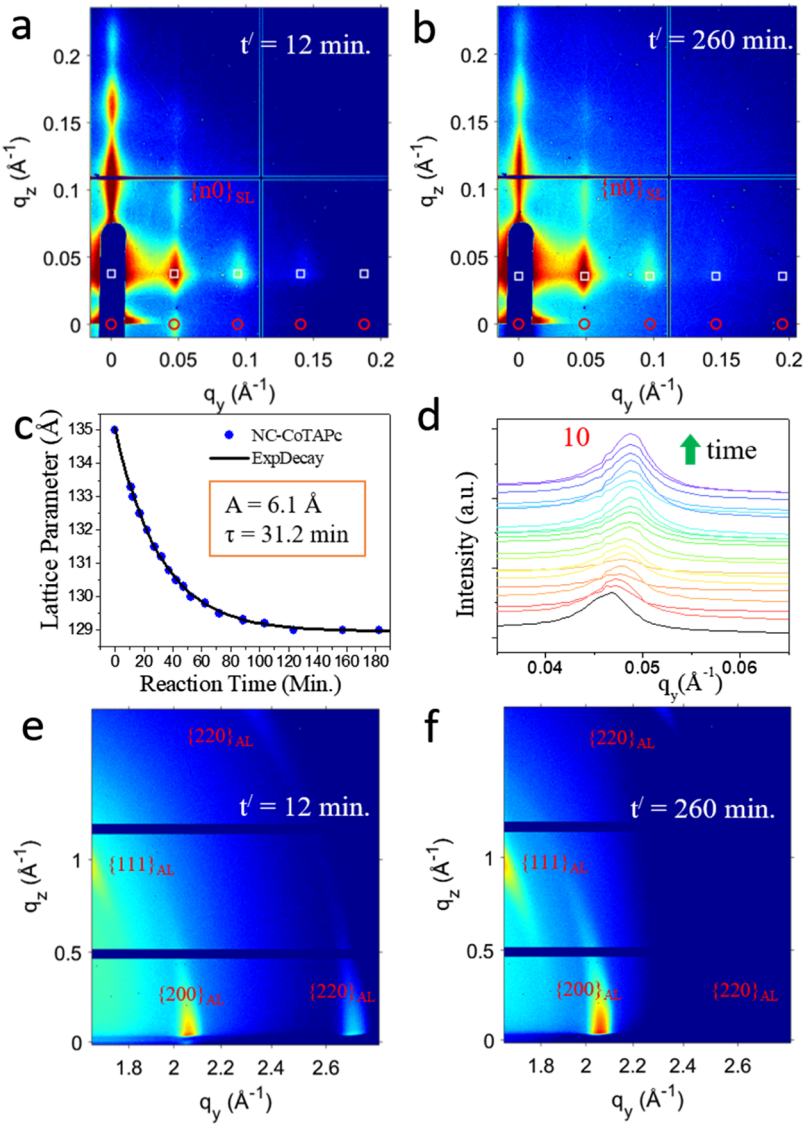

Figure 2. CoTAPc-induced assembly of cubic PbS NCs. GISAXS patterns of the NCs for a waiting period of (a) 12 and (b) 260 min after the injection of CoTAPc/DMSO solution into the bulk acetonitrile liquid. The red circles and white boxes are the simulated diffraction patterns considering a square SL (space group: *P4mm*) along the in-plane direction. (c) Temporal evolution of the lattice parameter of the square unit cell, extracted by fitting each image with varied unit cell parameters with elapsed time. (d) In-plane line profiles along q_y through the $\{n_0\}$ truncation rods of the GISAXS patterns obtained during ligand exchange. Peak intensities have been scaled up for clarity. GIXD patterns of the NCs on the acetonitrile surface for an elapsed time of (e) 12 and (f) 260 min after injecting the CoTAPc DMSO solution into the bulk liquid.

and used as received. The structural formulae are shown in Figure S8.

Formation of NC Films at the Liquid/Air Interface and Ligand Exchange. At first, the nitrogen-flushed chamber is filled up to 5 mm below the window edge with acetonitrile. 200 μL of the 2.5 μM NC solution in a mixture of 1:2 hexane (97%, extra dry, nitrogen flushed, Acros Organics) to octane (99+%, extra dry, nitrogen flushed, Acros Organics) is dispersed on top of the acetonitrile at a rate of 1 mL/min. A nanoparticle film forms within a few seconds.[23] After beam alignment onto the liquid surface, the measurements before ligand injection are done.

After the investigations of the OA-capped NC film are finished, a 1 mg/mL solution in dimethyl sulfoxide (DMSO) of Co/CuTAPc is injected into the bulk acetonitrile liquid. The start of the injection process marks the time zero of our experiment. The subphase height was adjusted about every 15 min. For better control on the experiment, all the injection or dispersion processes are performed with the help of a syringe pump.

In Situ GISAXS and GIXD. Simultaneous GISAXS and GIXD were performed at the European Synchrotron Radiation Facility (ESRF) in Grenoble, France at the ID10 beamline. The X-ray beam energy was set to 10 keV by using a Si(111) double crystal monochromator and focused with KB mirrors. The beam size was 15 μm × 250 μm ($V \times H$) at the exit slit of the beamline. The X-ray grazing incidence angle was 0.2° with respect to the plane of the liquid surface. The GISAXS signals were collected with a MAXIPIX detector (28 mm × 28 mm), with a pixel size of 55 × 55 μm^2. The detector was placed at a distance of 567 mm determined by an Ag-behenate reference. The each GISAXS images were collected over 5 s of exposure time. The GIXD images were collected with a Pilatus 300 K detector, having a pixel size of 172 × 172 μm^2, placed at a

DOI: 10.1021/acs.jpcc.8b11518
J. Phys. Chem. C 2019, 123, 1519−1526

distance of 264 mm. Each GIXD image was collected over 5 s of exposure time simultaneously with the GISAXS images.

Characterization. Scanning electron microscopy (STEM, Hitachi SU 8030 microscope operating at 30 kV) measurements were performed to determine the SL structure. Raman spectra (Horiba Jobin Yvon Labram HR 800 spectrometer) were collected using a He:Ne laser (wavelength 633 nm) as an excitation source and a CCD-1024 × 256-OPEN-3S9 detector. The ligand-exchanged films were transferred onto commercially available bottom-gate, bottom-contact transistor substrates (Fraunhofer Institute for Photonic Microsystems, Dresden, Germany) with interdigitated Au electrodes of 10 mm width and 2.5 μm channel length. Two-probe electrical measurements were carried out using a Keithley 2634B dual-source measurement unit. The particle size distribution was determined from an ensemble of >400 NCs by transmission electron microscopy (TEM).

RESULTS

Self-Assembly of OA-Capped NCs on the Liquid Surface. Figure 1 shows in situ scattering patterns of the NCs after spreading them onto the acetonitrile/air interface, collected as a function of waiting period during their self-assembly. Representative GISAXS (geometry in Figure S1) patterns at the very beginning (2.5 min) and after 32 min of waiting time are presented in Figure 1a,b, whereas others during intermediate times are shown in the Supporting Information (Figure S2). The appearance of several in-plane truncation rods, positioned at integer multiple positions of the first rod (marked as 1st in Figure 1a) in all GISAXS patterns evidences the formation of a self-assembled square SL structure by the NCs which remain as square periodic for the rest of the self-assembly time. The diffraction peaks in the GISAXS patterns are fitted by the distorted wave Born approximation (DWBA) method,[26−29] considering a *P4mm* space group symmetry for the 2D square lattice. The lattice parameters are extracted from fitting the experimental peak positions in the line profiles (Figure 1c). We obtain an unaltered lattice parameter of $a = (13.5 \pm 0.05)$ nm which is also evident from the stable in-plane positions of the diffraction rods in the corresponding line profiles (Figure 1d). Only a small contraction of ∼0.1 nm has been observed within 12 min of self-assembly. The average coherent domain sizes of the SLs are estimated from the full width at half-maximum (fwhm) by Lorentzian fitting of the truncation rods in the time-resolved scattering profiles and found to be almost identical over the entire assembling period. The obtained domain size is about 122 nm, which corresponds to a 2D square array of approximately 10 × 10 NCs. Typical in situ GIXD patterns of the NCs during self-assembly on the acetonitrile surface at 2.5 and 32 min are presented in Figure 1e,f. The appearance of the 200 diffraction peaks along the in-plane direction and the 111 peak at the azimuthal position (∼35.3°) in the 2.5 min GIXD pattern (Figure 1e) indicates that all NCs within the SLs are oriented with a $[100]_{AL}$ axis perpendicular to the liquid surface. It is important to note that the 220 peak appears not only at 45° angular position (the relative angle between $\{100\}_{AL}$ and $\{110\}_{AL}$ atomic planes) but also along the in-plane direction. This can be rationalized with the presence of several oriented (0° ± 90°) domains (typical domain size ∼120 nm^2 and beam footprint ∼150 μm (H) × 25 mm (L)) with respect to the direct beam/other domains. We observed very similar diffraction peaks in the GIXD patterns (Figures 1f and S3) during the rest of the waiting period (∼32 min). The preferential atomic orientation of the NCs along the $[100]_{AL}$ axis is supported further by symmetric ($\theta_i = \theta_f$) X-ray diffraction (XRD) after lifting the SL film onto Si substrates (Figure S4). The GIXD results confirm that the NCs remain preferentially oriented during the self-assembly process. The sizes of the individual NCs are determined from the fwhm of the GIXD line profiles using the Scherrer formula,[30] which are found to be ∼11.8 nm for each case. During the self-assembly process, the fwhm of the GIXD profiles does not change with time. This suggests that there is no significant sintering or fusion of the NCs during the assembly process. An interparticle separation (surface to surface) of 2.0 nm is obtained by subtracting the NC size from the (super)lattice parameter (a), which is a typical length of an OA ligand.

Self-Assembly during Ligand Exchange with CoTAPc on the Liquid Surface. Simultaneous in situ GISAXS and GIXD measurements have been performed to monitor the structural change during ligand exchange of the self-assembled NCs (square SL) with CoTAPc on the acetonitrile surface. The typical GISAXS patterns after 8 min of the ligand injection and after a waiting period of 260 minutes are presented in Figure 2a,b. The patterns (taken every 3−5 min of interval) for intermediate times are provided in Video S1. The scattering patterns in the GISAXS images after ligand injection (Figure 2, Video S1) show a high resemblance with the patterns collected during self-assembly (Figure 1), indicating that the ligand exchange with CoTAPc does not noticeably alter the symmetry of the SL at the liquid/air interface. The scattering patterns in the GISAXS images are simulated and fitted by taking into account DWBA corrections. Each of them corresponds to a square SL structure with *P4mm* space group symmetry. The extracted lattice parameter as a function of elapsed time is presented in Figure 2c. The initial lattice parameter (13.6 nm) contracts to 12.9 nm due to ligand exchange during a t period of 260 min. The contraction of the SL parameter (δ) follows an exponential decay of

$$\delta = A \times \exp(-t/\tau) + \delta_f$$

as a function of elapsed time, where "A" is a constant, "δ_f" is the final N−N distance, "t" is the elapsed time, and "τ" is the time constant. The extracted parameters (δ_f, A, and τ_1) for the lattice contraction during cross-linking are 129 Å, 6.1 Å, and 31.2 min. The average coherent domain size of the SLs after complete ligand exchange is found to be about 115 nm. A size reduction of the domain by ∼7 nm can be attributed to a resultant contraction between the nearest neighbor nanoparticles during ligand exchange (considering a domain of 10 × 10 NCs, an average N−N contraction of 0.7 nm, for an array of 10 NCs contraction 0.7 × 9 = 6.3 nm). The lattice contraction (shift of the 100 peak to a higher q_y-value) is also evident in the extracted line profiles (Figure 2d) from the corresponding time-resolved scattering patterns. The GIXD patterns obtained from the same SL assembly after injecting the ligand for 12 and 260 min are presented in Figure 2e,f. For both cases, the 200 diffraction peak appears along the in-plane direction and the 111 peak at the azimuthal position (35.3°). There is no visible change in the diffraction peaks/patterns also in the GIXD images at the intermediate times (Video S1). This result suggests that the NCs remain in a $\{100\}_{AL}$-face up configuration within the SL with respect to the liquid surface during the whole period of the ligand exchange. Our symmetric ($\theta_i = \theta_f$) XRD results from the ligand-exchanged

DOI: 10.1021/acs.jpcc.8b11518
J. Phys. Chem. C 2019, 123, 1519−1526

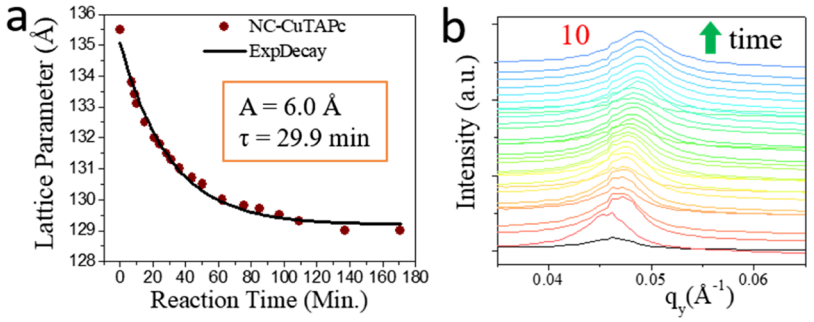

Figure 3. CuTAPc-induced assembly of cubic PbS NCs. (a) Temporal evolution of the lattice parameter of the 2D square unit cell, extracted by fitting each image. Scans were taken in intervals of 4−5 min. (b) In-plane GISAXS line profiles along q_y through the 10 truncation rods of the patterns obtained after the injection of CuTAPc/DMSO solution into the bulk acetonitrile liquid. Peak intensities have been scaled up for clarity.

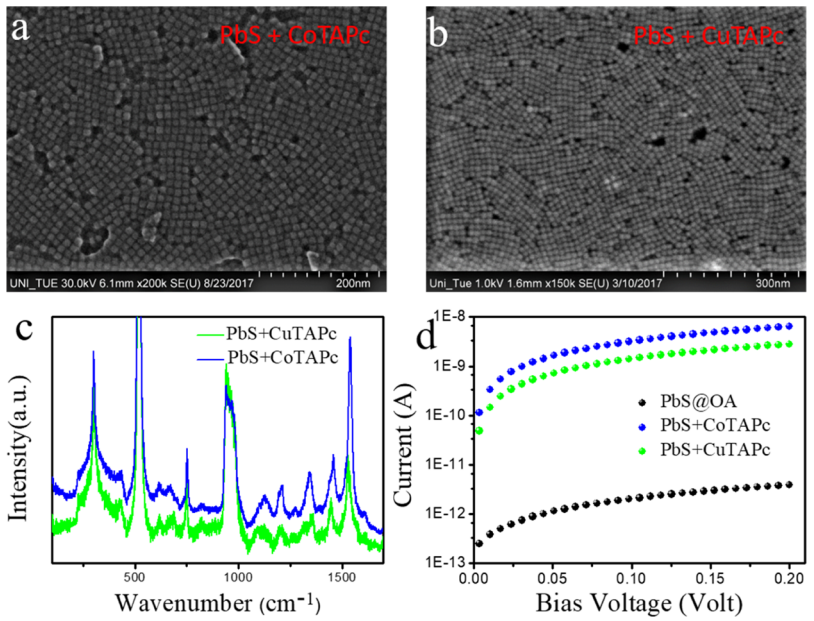

Figure 4. SEM image of PbS NCs coupled with (a) CoTAPc and (b) CuTAPc molecules showing square periodic domains. (c) Raman spectroscopy data after ligand exchange films. (d) Current−voltage (I−V) characteristics of PbS NC films: OA-capped (black); exchange film with CoTAPc (blue) and CuTAPc (green); the graph is plotted on a logarithmic scale for better comparison.

SL film after lifting onto Si substrates (Figure S4) also corroborate the preferentially oriented NCs with a $[100]_{AL}$ axis perpendicular to the substrate. We always observe similar fwhm of the first correlation peak. The in-plane sizes of the NCs are found to be ∼11.8 nm, which implies that there is no sintering or fusion of consecutive NCs during this ligand exchange.

Self-Assembly during Ligand Exchange with CuTAPc on the Liquid Surface. Similar grazing incidence X-ray scattering measurements have been performed to compare the ligand exchange mechanism with CuTAPc molecules. GISAXS and GIXD patterns taken in intervals of 4−5 min during NC assembly and ligand exchange are shown in Figures S5 and S6. The contraction of the SL parameter also follows a similar exponential decay (τ = 29.8 min) in the presence of CuTAPc ligands (Figure 3a,b). Likewise, a preferential orientation of the NCs within the SL, facing {100} upward with respect to the acetonitrile surface, is observed.

Ex Situ Characterization of the Ligand Exchanged Films. Figure 4a,b shows a typical real-space SEM image of the ligand-exchanged PbS NC films coupled with CoTAPc and CuTAPc molecules, obtained after transfer from the acetonitrile/air interface. The images clearly demonstrate that the NCs self-assemble into SLs with a square periodic order. Raman spectroscopy (Figure 4c) on the recovered exchanged films shows the presence of intense bands at wavenumbers >1000 cm^{-1}, which are a strong indication for the presence of the new Co/CuTAPc ligands on the surface of the NPs. It should be noted that we extensively washed the films with acetonitrile to remove excess/free ligand molecules. We compare the transport measurements of the ligand exchanged and self-assembled films in Figure 4d. The current−voltage (I−V) characteristics indicate an improvement of the current by 4 orders of magnitude for ligand exchanged film with respect to the native OA-capped PbS film.

DISCUSSION

We attempt a comparative discussion of our experimental results with a few other recent studies focused on in situ self-assembly or induced assembly of NCs at liquid/air interfaces. Recently, we monitored the real-time ligand-induced assembly of cuboctahedral PbS NC multilayers with tetrathiafulvalene dicarboxylate (TTFDA) by GISAXS.[23] We reported an isotropic contraction of the NC SL during self-assembly as

DOI: 10.1021/acs.jpcc.8b11518
J. Phys. Chem. C 2019, 123, 1519−1526

well as during the ligand-induced assembly process while conserving the bcc SL symmetry. In contrast, in the present work, we use cubic NCs to form a monolayer SL on the acetonitrile surface and employed disk-like tetraamino-phthalocyanine (CoTAPc and CuTAPc) molecules for ligand exchange. We observed a square SL formation before and after ligand exchange. Geuchies et al. recently found that PbSe NCs self-assemble into square SLs from a quasi-hexagonal superstructure on an ethylene glycol surface.[33] They also observed atomically coherent NC SLs formed during solvent evaporation. The phenomena were attributed to "atomic necking" between the $\{100\}_{AL}$ facets of NCs during solvent evaporation. In contrast, we have not seen any structural (symmetry) transformation of the SLs either during self-assembly or during both ligand exchange processes. Rather, the cubic NCs are aligned preferentially with respect to the acetonitrile surface from the very beginning of the experiment (1.7 min) and remain oriented throughout the assembly processes. van der Stam et al. observed that bifrustum-shaped ZnS NCs form hexagonal SLs on the ethylene glycol−air interface with their {002} facets preferentially adhering to the interface.[34] An in-plane contraction of the SL of about 1.5 nm has been reported during self-assembly with adding OA, while 1.8 nm without adding any OA. The authors attributed this to the buckling of ligands during solvent evaporation.

Here, we extend the discussion on the formation mechanism of conductive iso-oriented mesocrystalline superstructures of NCs with possible explanations. In our recent work, by using cuboctahedral NCs (6.8 nm diameter), we obtained a bcc SL during self-assembly through an overall contraction of 5% and did not determine the atomic coherence of the NCs in the SLs.[23] We attributed the contraction to a combined effect of solvent vapor conditions and capillary waves.[23] In the present study, we used a liquid cell having a small outlet for instant release of solvent vapors and increased the size of the NCs (cubic shape; 11.8 nm) to reduce capillary effects acting on the interface/NCs. As a consequence, we have not seen any kind of buckling but only a small contraction (∼0.1 nm) during self-assembly via carrier-solvent evaporation. Our GIXD data shows that the NCs not only assemble into a square SL but also align with their $\{100\}_{AL}$ facets parallel to the liquid surface (just after injection (∼2 min)), without any further change in the SL structure, symmetry, or orientation. The strong out-of-plane attraction of the acetonitrile substrate on the {100} facets and the in-plane attraction between $\{100\}_{AL}$−$\{100\}_{AL}$ facets of the alternating NCs other than the steric repulsions of the OA ligands presumably keep the NCs oriented with respect to the liquid surface.

Instead of rodlike TTFDA molecules (∼1.1 nm in length), exhibiting two carboxylic acid functional groups, in the present case, we use two disk-shaped tetraamino-phtalocyanine molecules of similar sizes (CoTAPc and CuTAPc) to obtain conductive PbS nanostructures. Both are fully conjugated, small and rigid OSC molecules with a sp^2-hybridized carbon backbone and have four reactive $-NH_2$ groups. A significant contraction of 0.7 nm (obtained from GISAXS) after ligand exchange indicates that Co/Cu-TAPc at least partially replaces OA as the ligand, suggesting that these molecules have a higher binding strength to PbS than OA. The preferential atomic alignment and contraction of the SL along the $[100]_{SL}$ direction indicates that OA is predominantly replaced from the $\{100\}_{AL}$ facets of PbS. This can be rationalized with the fact that OA binds to these facets as the neutral acid, which is a weak Lewis base, and is much easily replaced than the corresponding carboxylate on the $\{111\}_{AL}$ facets.[35] The small difference in time constant for two phthalocyanines corresponds to different reactions and/or diffusion rates of the molecules in the subphase, which is probably due to the presence of different metal centers. Finally, the phthalocyanine-coupled NCs are likely to exhibit structural rigidity in the ligand shell and cannot undergo further structural changes easily once the interparticle distance is on the order of one Co/Cu-TAPc molecule (1.4 nm). For both cases, the quadratic SLs contract until they reach a minimum interparticle distance, and the reduction of SL parameters follows exponential decay curves with almost identical rates. The similar interparticle spacing after ligand exchange confirms the presence of similar size molecules in between the adjacent NCs. The enhancement of the electrical conductivity by 4 orders of magnitude (refer Figure 4d) for ligand-exchanged films is attributed to the formation of conductive PbS NC SLs by cross-linking with the phthalocyanine molecules.[24]

CONCLUSIONS

In summary, we have monitored the structural evolution during self-assembly followed by ligand exchange of a cubic PbS NC SL on the acetonitrile surface. We used the disk-shaped cross-linkers CoTAPc and CuTAPc to exchange the native OA ligands and investigated the in situ structural changes of the SLs. We determine the SL parameters from the scattering patterns by fitting the diffraction peaks and monitor the orientation of the ALs of NCs within the SL. We observe an exponential ($\tau \approx 30$ min) contraction of the in-plane SL parameters during ligand exchange, preserving the symmetry (S. G. *P4mm*) of the 2D square lattice. A resultant lattice contraction of 5% is attributed to the replacement of the native surface ligands (OA) by the smaller Co/CuTAPc cross-linkers. Just after the injection of the cubic NCs, they orient preferentially with respect to the liquid surface and remain oriented such that $\{100\}_{AL}$ facet points upward also during ligand exchange. Using this process, it is possible to produce long-range ordered, iso-oriented mesocrystalline conductive SLs of NCs.

ASSOCIATED CONTENT

Supporting Information

The Supporting Information is available free of charge on the ACS Publications website at DOI: 10.1021/acs.jpcc.8b11518.

The following files are available free of charge. Schematic diagram of the setup used for GISAXS and GIXD experiments of NC assembly at the solid/air interface, GISAXS patterns of the NCs for different waiting periods (times are in the top-right corner of each images) after injection onto the acetonitrile surface and during solvent evaporation, GIXD patterns of the NCs for different waiting periods (times are in the top-right corner of each images) after injecting them onto the acetonitrile surface through solvent evaporation, symmetric X-ray diffraction (SXRD scanning at $\theta_i = \theta_f$ geometry) profiles of the PbS@OA and PbS NCs functionalized with CuTAPc showing the presence of only {200} diffraction peaks, typical GISAXS patterns of the NCs for a waiting period of (a) 07 and (b) 171 min after the injection of CuTAPc in DMSO solution into the bulk acetonitrile liquid, typical GIXD patterns of the

DOI: 10.1021/acs.jpcc.8b11518
J. Phys. Chem. C 2019, 123, 1519−1526

NCs on an acetonitrile surface for an elapsed time of (a) 07 and (b) 171 min after injecting the CuTAPc DMSO solution into the bulk liquid, (a) TEM images of cubic PbS NCs and (b) their size distribution, and structural formula of Co/CuTAPc with M = Co /Cu as the metal center (PDF)

Patterns (taken every 3−5 min of interval) for intermediate times (ZIP)

AUTHOR INFORMATION

Corresponding Authors

*E-mail: santanu.maiti@uni-tuebingen.de (S.M.).
*E-mail: frank.schreiber@uni-tuebingen.de (F.S.).
*E-mail: marcus.scheele@uni-tuebingen.de (M.S.).

ORCID

Santanu Maiti: 0000-0003-1491-6688
Frank Schreiber: 0000-0003-3659-6718
Marcus Scheele: 0000-0002-2704-3591

Notes

The authors declare no competing financial interest.

ACKNOWLEDGMENTS

This work was supported by the DFG under grants SCHE1905/3, SCHE1905/4, and SCHR700/25. We thank the European Synchrotron Radiation Facility (ESRF), Grenoble, France, for enabling X-ray scattering experiments at beamline ID10. Elke Nadler, Institute of Physical and Theoretical Chemistry, University of Tübingen, is acknowledged for performing SEM/STEM measurements using a Hitachi SU 8030 SEM which was funded by the DFG under contract INST 37/829-1 FUGG, partially. We also acknowledge the fruitful discussion with A. André and O. Konovalov on the project.

REFERENCES

(1) Bigioni, T. P.; Lin, X.-M.; Nguyen, T. T.; Corwin, E. I.; Witten, T. A.; Jaeger, H. M. Kinetically Driven Self Assembly of Highly Ordered Nanoparticle Monolayers. *Nat. Mater.* **2006**, *5*, 265−270.

(2) Rabani, E.; Reichman, D. R.; Geissler, P. L.; Brus, L. E. Drying-Mediated Self-Assembly of Nanoparticles. *Nature* **2003**, *426*, 271−274.

(3) Smilgies, D.-M.; Heitsch, A. T.; Korgel, B. A. Stacking of Hexagonal Nanocrystal Layers during Langmuir-Blodgett Deposition. *J. Phys. Chem. B* **2012**, *116*, 6017−6026.

(4) Vegso, K.; Siffalovic, P.; Majkova, E.; Jergel, M.; Benkovicova, M.; Kocsis, T.; Weis, M.; Luby, S.; Nygård, K.; Konovalov, O. Nonequilibrium Phases of Nanoparticle Langmuir Films. *Langmuir* **2012**, *28*, 10409−10414.

(5) Wang, M. X.; Seo, S. E.; Gabrys, P. A.; Fleischman, D.; Lee, B.; Kim, Y.; Atwater, H. A.; Macfarlane, R. J.; Mirkin, C. A. Epitaxy: Programmable Atom Equivalents Versus Atoms. *ACS Nano* **2016**, *11*, 180−185.

(6) Dai, Y.; Lin, B.; Meron, M.; Kim, K.; Leahy, B.; Witten, T. A.; Shpyrko, O. G. Synchrotron X-ray Studies of Rapidly Evolving Morphology of Self-Assembled Nanoparticle Films under Lateral Compression. *Langmuir* **2013**, *29*, 14050−14056.

(7) You, S. S.; Heffern, C. T. R.; Dai, Y.; Meron, M.; Henderson, J. M.; Bu, W.; Xie, W.; Lee, K. Y. C.; Lin, B. Liquid Surface X-ray Studies of Gold Nanoparticle-Phospholipid Films at the Air/Water Interface. *J. Phys. Chem. B* **2016**, *120*, 9132−9141.

(8) André, A.; Zherebetskyy, D.; Hanifi, D.; He, B.; Khoshkhoo, M. S.; Jankowski, M.; Chassé, T.; Wang, L.-W.; Schreiber, F.; Salleo, A.; et al. Toward Conductive Mesocrystalline Assemblies: PbS Nanocrystals Cross-Linked with Tetrathiafulvalene Dicarboxylate. *Chem. Mater.* **2015**, *27*, 8105−8115.

(9) Dong, A.; Jiao, Y.; Milliron, D. J. Electronically Coupled Nanocrystal Superlattice Films by in Situ Ligand Exchange at the Liquid-Air Interface. *ACS Nano* **2013**, *7*, 10978−10984.

(10) Scheele, M.; Brütting, W.; Schreiber, F. Coupled Organic-Inorganic Nanostructures (COIN). *Phys. Chem. Chem. Phys.* **2015**, *17*, 97−111.

(11) Bian, K.; Choi, J. J.; Kaushik, A.; Clancy, P.; Smilgies, D.-M.; Hanrath, T. Shape-Anisotropy Driven Symmetry Transformations in Nanocrystal Superlattice Polymorphs. *ACS Nano* **2011**, *5*, 2815−2823.

(12) Boles, M. A.; Engel, M.; Talapin, D. V. Self-Assembly of Colloidal Nanocrystals: From Intricate Structures to Functional Materials. *Chem. Rev.* **2016**, *116*, 11220−11289.

(13) Vanmaekelbergh, D. Self-Assembly of Colloidal Nanocrystals as Route to Novel Classes of Nanostructured Materials. *Nano Today* **2011**, *6*, 419−437.

(14) Zaluzhnyy, I. A.; Kurta, R. P.; André, A.; Gorobtsov, O. Y.; Rose, M.; Skopintsev, P.; Besedin, I.; Zozulya, A. V.; Sprung, M.; Schreiber, F.; et al. Quantifying Angular Correlations between the Atomic Lattice and the Superlattice of Nanocrystals Assembled with Directional Linking. *Nano Lett.* **2017**, *17*, 3511−3517.

(15) Weidman, M. C.; Smilgies, D.-M.; Tisdale, W. A. Kinetics of the Self-Assembly of Nanocrystal Superlattices Measured by Real-Time in situ X-ray Scattering. *Nat. Mater.* **2016**, *15*, 775−781.

(16) Maiti, S.; Sanyal, M. K.; Varghese, N.; Satpati, B.; Dasgupta, D.; Daillant, J.; Carriere, D.; Konovolov, O.; Rao, C. N. R. Formation of Single-Crystalline CuS at the Organic-Aqueous Interface. *J. Phys.: Condens. Matter* **2013**, *25*, 395401.

(17) Khoshkhoo, M. S.; Maiti, S.; Schreiber, F.; Chassé, T.; Scheele, M. Surface Functionalization with Copper Tetraaminophthalocyanine Enables Efficient Charge Transport in Indium Tin Oxide Nanocrystal Thin Films. *ACS Appl. Mater. Interfaces* **2017**, *9*, 14197−14206.

(18) Kosif, I.; Kratz, K.; You, S. S.; Bera, M. K.; Kim, K.; Leahy, B.; Emrick, T.; Lee, K. Y. C.; Lin, B. Robust Gold Nanoparticle Sheets by Ligand Cross-Linking at the Air-Water Interface. *ACS Nano* **2017**, *11*, 1292−1300.

(19) Lazarenkova, O. L.; Balandin, A. A. Miniband Formation in a Quantum Dot Crystal. *J. Appl. Phys.* **2001**, *89*, 5509−5515.

(20) Whitham, K.; Yang, J.; Savitzky, B. H.; Kourkoutis, L. F.; Wise, F.; Hanrath, T. Charge Transport and Localization in Atomically Coherent Quantum Dot Solids. *Nat. Mater.* **2016**, *15*, 557−563.

(21) Cao, Y.; Stavrinadis, A.; Lasanta, T.; So, D.; Konstantatos, G. The Role of Surface Passivation for Efficient and Photostable PbS Quantum Dot Solar Cells. *Nat. Energy* **2016**, *1*, 16035.

(22) de Arquer, F. P. G.; Armin, A.; Meredith, P.; Sargent, E. H. Solution-Processed Semiconductors for Next-Generation Photodetectors. *Nat. Rev. Mater.* **2017**, *2*, 16100.

(23) Maiti, S.; André, A.; Banerjee, R.; Hagenlocher, J.; Konovalov, O.; Schreiber, F.; Scheele, M. Monitoring Self-Assembly and Ligand Exchange of PbS Nanocrystal Superlattices at the Liquid/Air Interface in Real Time. *J. Phys. Chem. Lett.* **2018**, *9*, 739−744.

(24) André, A.; Theurer, C.; Lauth, J.; Maiti, S.; Hodas, M.; Khoshkhoo, M. S.; Kinge, S.; Meixner, A. J.; Schreiber, F.; Siebbeles, L. D. A.; et al. Structure, Transport and Photoconductance of PbS Quantum Dot Monolayers Functionalized with a Copper Phthalocyanine Derivative. *Chem. Commun.* **2017**, *53*, 1700−1703.

(25) Jung, S.-H.; Choi, J.-H.; Yang, S.-M.; Cho, W.-J.; Ha, C.-S. Syntheses and Characterization of Soluble Phthalocyanine Derivatives for Organic Electroluminescent Devices. *Mater. Sci. Eng., B* **2001**, *85*, 160−164.

(26) Jiang, Z. GIXSGUI: a MATLAB Toolbox for Grazing-Incidence X-ray Scattering Data Visualization and Reduction, and Indexing of Buried Three-Dimensional Periodic Nanostructured Films. *J. Appl. Crystallogr.* **2015**, *48*, 917−926.

(27) Tate, M. P.; Urade, V. N.; Kowalski, J. D.; Wei, T.-c.; Hamilton, B. D.; Eggiman, B. W.; Hillhouse, H. W. Simulation and Interpretation of 2D Diffraction Patterns from Self-Assembled

DOI: 10.1021/acs.jpcc.8b11518
J. Phys. Chem. C 2019, 123, 1519−1526

Nanostructured Films at Arbitrary Angles of Incidence: From Grazing Incidence (above the Critical Angle) to Transmission Perpendicular to the Substrate. *J. Phys. Chem. B* **2006**, *110*, 9882−9892.
(28) Sinha, S. K.; Sirota, E. B.; Garoff, S.; Stanley, H. B. X-Ray and Neutron-Scattering from Rough Surfaces. *Phys. Rev. B: Condens. Matter Mater. Phys.* **1988**, *38*, 2297−2311.
(29) Renaud, G.; Lazzari, R.; Leroy, F. Probing Surface and Interface Morphology with Grazing Incidence Small Angle X-Ray Scattering. *Surf. Sci. Rep.* **2009**, *64*, 255−380.
(30) Maiti, S.; Sanyal, M. K.; Jana, M. K.; Runge, B.; Murphy, B. M.; Biswas, K.; Rao, C. N. R. Evidence of Contact Epitaxy in the Self-Assembly of HgSe Nanocrystals Formed at a Liquid-Liquid Interface. *J. Phys.: Condens. Matter* **2017**, *29*, 095101.
(31) Weidman, M. C.; Yager, K. G.; Tisdale, W. A. Interparticle Spacing and Structural Ordering in Superlattice PbS Nanocrystal Solids Undergoing Ligand Exchange. *Chem. Mater.* **2014**, *27*, 474−482.
(32) Jung, S.-H.; Choi, J.-H.; Yang, S.-M.; Cho, W.-J.; Ha, C.-S. Syntheses and Characterization of Soluble Phthalocyanine Derivatives for Organic Electroluminescent Devices. *Mater. Sci. Eng., B* **2001**, *85*, 160−164.
(33) Geuchies, J. J.; van Overbeek, C.; Evers, W. H.; Goris, B.; de Backer, A.; Gantapara, A. P.; Rabouw, F. T.; Hilhorst, J.; Peters, J. L.; Konovalov, O.; et al. In Situ Study of the Formation Mechanism of Two-Dimensional Superlattices from PbSe Nanocrystals. *Nat. Mater.* **2016**, *15*, 1248−1254.
(34) van der Stam, W.; Rabouw, F. T.; Vonk, S. J. W.; Geuchies, J. J.; Ligthart, H.; Petukhov, A. V.; Donega, C. d. M. Oleic Acid-Induced Atomic Alignment of ZnS Polyhedral Nanocrystals. *Nano Lett.* **2016**, *16*, 2608−2614.
(35) Zherebetskyy, D.; Wang, L.-W. In-Gap States in Electronic Structure of Nonpolar Surfaces of Insulating Metal Oxides. *Adv. Mater. Interfaces* **2014**, *1*, 1300131.

DOI: 10.1021/acs.jpcc.8b11518
J. Phys. Chem. C 2019, 123, 1519−1526